

Nonabelian Cut Diagrams

C. S. Lam [†] *

*Department of Physics, McGill University,
3600 University St., Montreal, P.Q., Canada H3A 2T8*

Abstract

Symmetrization of bosonic wave functions produces bunching and low temperature phenomena like Bose-Einstein condensation, superfluidity, superconductivity, as well as laser. Since probability is conserved, one might expect such bunchings at one place would lead to a depletion or a destructive interference at another place. This indeed takes place in high-energy scatterings, leading to cancellations between Feynman diagrams with permuted (real or virtual) boson lines. It is such cancellation that allow the Froissart bound to be obeyed, and the meson-baryon amplitudes in large- N_c QCD to be consistent. These lectures review the derivation and some of the applications of *nonabelian cut diagrams*, which are resummation of Feynman diagrams, but with these interference effects explicitly incorporated. Unlike the traditional method where cancellations occur between Feynman diagrams, making it necessary to compute each diagram to subleading orders, destructive interference has been taken care of from the start in nonabelian cut diagrams. No further cancellation takes place, so each nonabelian cut diagram may be computed only in the leading order.

[†] Lectures given at the First Asia Pacific Workshop on Strong Interactions, Taipei. August 1st to 27th, 1996.

* Email: Lam@physics.mcgill.ca

TABLE OF CONTENTS

1. Preliminaries
 1. Introduction
 2. Conventions
 3. Feynman rules
 4. Color algebra
2. High-Energy Elastic Scattering
 1. Energy dependence and Regge poles
 2. QED to $O(g^6)$
3. Abelian Cut Diagrams
 1. Factorization formula
 2. Sum of QED s -channel-ladder diagrams
 3. Other sum rules
4. Nonabelian Cut Diagrams
 1. Multiple commutator formula
 2. Folding formula
5. Quark-Quark Scattering to $O(g^6)$
 1. Color factors
 2. Sum of Feynman diagrams
 3. Sum of nonabelian cut diagrams
6. Multiple Reggeons and QCD
 1. The reggeized factorization hypothesis
 2. BFKL equation and unitarity
 3. Nonabelian cut diagrams vs Feynman diagrams
 4. s -channel-ladder diagrams
7. References

1 PRELIMINARIES

1.1 Introduction

The symmetrization of bosonic wave functions leads to an effective attraction. At low temperatures this constructive interference gives rise to the Bose-Einstein condensation, superfluidity of Helium, and superconductivity, as well as laser.

Probability is conserved. If there is a concentration of wave function at one place then there is presumably a depletion at another. How can one observe this depletion, or destructive interference? It turns out that this can be seen in high energy processes. The effect is not as dramatic as the low-temperature constructive interference processes, but its presence is absolutely necessary to render theoretical consistency, as we shall see.

A general discussion of this interference can be found in Secs. 3 and 4. The interference effect can be incorporated in our calculations by using the the *multiple commutator formula* [1] and the *nonabelian cut diagrams* [2]. These cut diagrams may be considered as resummations of Feynman diagrams where the interference of the identical bosons in the diagrams, whether real or virtual, has been explicitly accounted for at the very first step, the step of drawing the diagrams before any computation begins. With the interference thus included, subsequent cancellations are not needed and will not occur. In contrast, if as usual Feynman diagrams are used, substantial amount of delicate cancellations between diagrams will occur at a later stage as a result of such destructive interference. This is often much more difficult to calculate as will be elaborated below.

A fairly dramatic example of this can be found in the QCD theory with a large number of color ($N_c \gg 1$). Its n -meson tree amplitude in the one-baryon sector, *viz.*, meson-baryon scattering producing $n-1$ mesons in the final state, depends on N_c as $N_c^{1-\frac{1}{2}n}$ [3]. In particular, taking $n = 1$, this shows that the meson-baryon Yukawa coupling constant go like $\sqrt{N_c}$. Since the baryon propagators are of order unity, individual Feynman tree diagrams will go like $N_c^{\frac{1}{2}n}$, which is $n-1$ powers of N_c larger than what the full amplitude should be. Unless a huge cancellation occurs when we sum up the $n!$ Feynman diagrams, the theory will not be consistent [4]! Such cancellation indeed occurs, it is a manifestation of the destructive interference mentioned earlier, but to see how that works directly using Feynman diagram is very difficult task. Not so with the nonabelian cut diagrams [5] because the interference effects leading to the cancellations have already been built in. We will not pursue this subject further here because it is a bit outside of the scope of this workshop.

What we will discuss is destructive interference in high-energy elastic scattering taking place in loops, where identical bosons are present in the intermediate states for the interference to take place. Individual Feynman diagrams with many loops often contain high powers of $\int_{m^2/\sqrt{s}} d\omega/\omega \sim \ln s$ [6, 7, 8, 9]. If not cancelled, the Froissart bound would be violated. When Feynman diagrams are summed, such offending $\ln s$ do get cancelled [6] as a result of the destructive interference mentioned earlier. However, it is difficult to see how this happens in traditional calculations for two reasons. First, one has to do a lot of

virtual work to compute terms that eventually get cancelled. Second and more seriously, such computations can usually be carried out only in the leading-log approximation. If these leading powers of $\ln s$ are cancelled out, then one needs to compute the subleading, the sub-subleading (etc.) terms in order to obtain a non-zero finite result at the end. Such tasks are often impossible except in very low orders. Again, the nonabelian cut diagrams bypass these difficulties [2, 10, 11] because the destructive interference effect has been taken care of before any computation even begins.

1.2 Conventions

We shall adopt the following conventions for the metric $g^{\mu\nu}$, the Dirac matrix γ^μ , and the Dirac spinor u :

$$\begin{aligned} g^{\mu\nu} &= (+ - - -)_{diag} \\ \{\gamma^\mu, \gamma^\nu\} &= 2g^{\mu\nu} \\ \bar{u}u &= 2M . \end{aligned} \tag{1.1}$$

The plane-wave states are normalized covariantly,

$$\langle \vec{p}' | \vec{p} \rangle = (2\pi)^3 (2p^0) \delta^3(\vec{p}' - \vec{p}) , \tag{1.2}$$

the S -matrix is related to the covariant T -matrix by the formula

$$S_{fi} = \mathbf{1}_{fi} + (2\pi)^4 i \delta^4(\dots) T_{fi} , \tag{1.3}$$

where $\delta^4(\dots)$ is the overall energy-momentum conservation δ -function, and the unitarity relation is given by

$$-\frac{i}{2} (T_{fi} - T_{fi}^*) = \text{Im} (T_{fi}) = \frac{1}{2} \sum_n \int T_{fn}^* d\Phi_n T_{ni} , \tag{1.4}$$

in which the expression for the n -body invariant phase space is

$$\int d\Phi_n = \int \prod_{i=1}^n \left(\frac{1}{(2\pi)^3} \frac{d^3 p'_i}{2p'_i{}^0} \right) (2\pi)^4 \delta^4(\dots) . \tag{1.5}$$

For elastic scattering with initial momenta p_i and final momenta p'_i , momentum conservation dictates that $p_1 + p_2 = p'_1 + p'_2$. The Mandelstam variables are $s = (p_1 + p_2)^2$, $t = (p_1 - p'_1)^2$, and $u = (p_1 - p'_2)^2$; they are related by $s + t + u = 2(M_1^2 + M_2^2)$. \sqrt{s} is the centre-of-mass energy, and $\Delta = \sqrt{-t}$ is the momentum transfer. We shall be concerned with situations where s is much larger than $-t$ and M_i^2 . The elastic cross-section is related to the elastic amplitude T_{fi} by

$$\int d\sigma = \int \frac{1}{2s} |T_{fi}|^2 d\Phi_2 = \frac{1}{16\pi s^2} \int |T_{fi}|^2 dt , \tag{1.6}$$

and the total cross-section is given by unitarity to be

$$\sigma_{tot} = \frac{1}{s} \text{Im}(T_{ii}) . \tag{1.7}$$

1.3 Feynman Rules

The Feynman rules for the T -matrix elements that will be needed are the following.

- Quark propagator: $(M + \gamma \cdot p)/(p^2 - M^2 + i\epsilon)$
- Gluon propagators in the Feynman gauge: $-g^{\mu\nu}/(p^2 + i\epsilon)$
- Quark-gluon vertex: $gt_a\gamma^\alpha$
- Triple-gluon vertex: $g(if_{abc})\{g^{\alpha\beta}(p_1 - p_2)^\gamma + g^{\beta\gamma}(p_2 - p_3)^\alpha + g^{\gamma\alpha}(p_3 - p_1)^\beta\}$
- Four-gluon vertex: $g^2\{f_{abe}f_{cde}(g^{\alpha\gamma}g^{\beta\delta} - g^{\alpha\delta}g^{\beta\gamma}) + f_{ace}f_{bde}(g^{\alpha\beta}g^{\gamma\delta} - g^{\alpha\delta}g^{\beta\gamma}) + f_{ade}f_{bce}(g^{\alpha\beta}g^{\delta\gamma} - g^{\alpha\gamma}g^{\delta\beta})\}$
- External wave functions: $\epsilon_\lambda^*(p), \epsilon_\lambda(p), \bar{u}_\lambda(p), u_\lambda(p)$
- Loop integration: $i \int d^4q/(2\pi)^4$
- Other factors: an overall minus sign, a minus sign per fermion loop, and symmetry factors.

1.4 Color Algebra

The $SU(N_c)$ color matrices t_a obeys the commutation relation

$$[t_a, t_b] = if_{abc}t_c . \quad (1.8)$$

The structure constants satisfy the sum rules

$$f_{abc}f_{abd} = N_c\delta_{cd}, \quad i^3 f_{adg}f_{bed}f_{cge} = i\frac{N_c}{2}f_{abc} \equiv icf_{abc} . \quad (1.9)$$

See Fig. 1 for a graphical representation of (1.8) and (1.9).

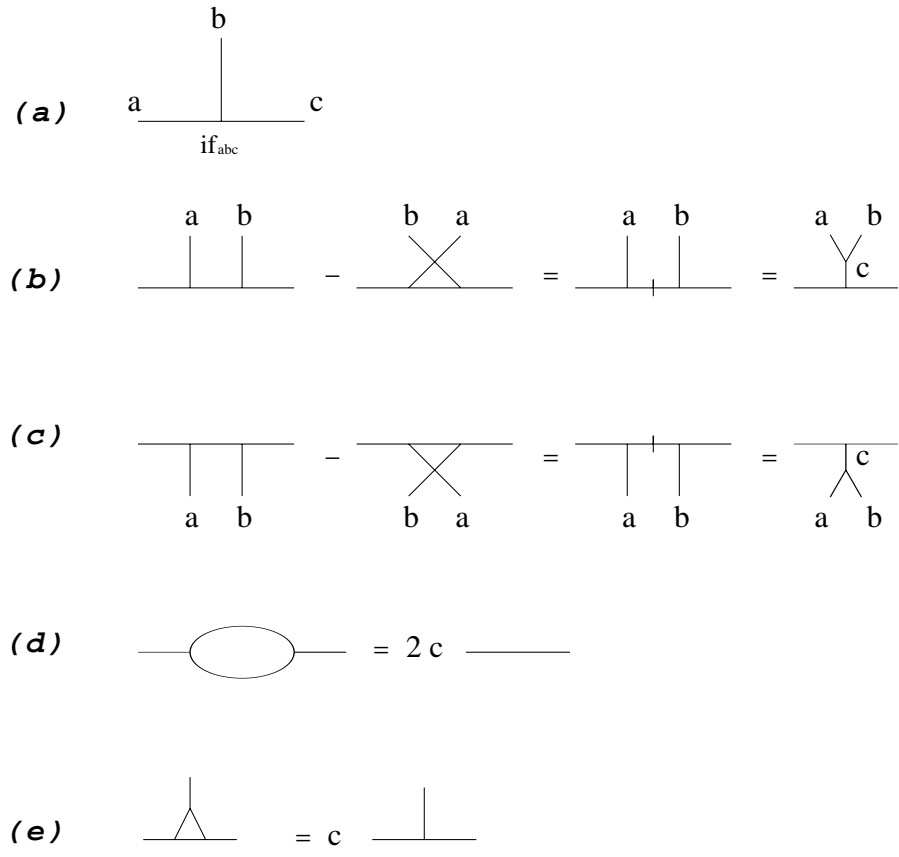


Figure 1: Graphical representation of the color-matrix relations (1.8) and (1.9).

2 HIGH-ENERGY ELASTIC SCATTERING

2.1 s -Dependence and Regge Poles

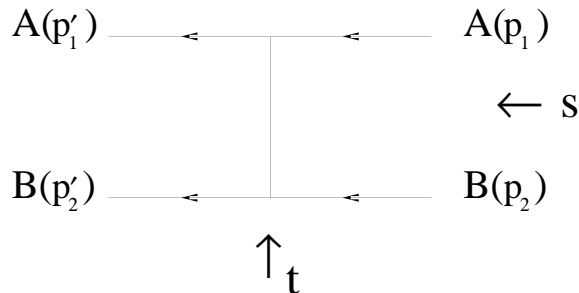


Figure 2: An elastic scattering process $A + B \rightarrow A + B$.

Consider the tree diagram in Fig. 2 for the elastic process $A + B \rightarrow A + B$. For simplicity we shall assume A and B to have the same mass. If all the particles are scalars then the T-matrix amplitude is $-g^2/t$ and is energy independent. On the other hand, if the exchange particle C is a photon, then the vertices add on an additional factor $\simeq -(2p_1) \cdot (2p_2) \simeq -2s$, now the amplitude grows linearly with s . In general, the amplitude grows like s^ℓ if the spin of the exchanged particle C is ℓ . To see that, analytically continue the amplitude to the physical region of the t -channel process $B + \bar{B} \rightarrow \bar{A} + A$, where $t > 0, s < 0, u < 0$. In its CM system, the total angular momentum is ℓ , so the amplitude is proportional to $P_\ell(\cos \theta_t)$, where θ_t is the CM scattering angle for this process and it is related to s and u by

$$s = -\frac{t}{2}(1 - \cos \theta_t), \quad u = -\frac{t}{2}(1 + \cos \theta_t). \quad (2.1)$$

We can now analytically continue back to the physical region of the s -channel process and examine the limit when $s \rightarrow \infty$. Since

$$P_\ell(z) \sim z^\ell, \quad (\text{Re} \ell > -\frac{1}{2}) \quad (2.2)$$

for large $z_t \equiv -\cos \theta_t \sim s$, the amplitude grows like s^ℓ as claimed.

What if we have a complicated diagram so that the t -channel angular momentum is not fixed? Then the amplitude is given by a partial-wave expansion

$$T(s, t) = \sum_\ell a_\ell(t)(2\ell + 1)P_\ell(z_t), \quad (2.3)$$

say with some ‘mean’ angular momentum $\bar{\ell} \equiv \alpha(t)$. If the spread of angular momentum is small, one might expect simply by interpolation that the amplitude still grows like $s^{\alpha(t)}$.

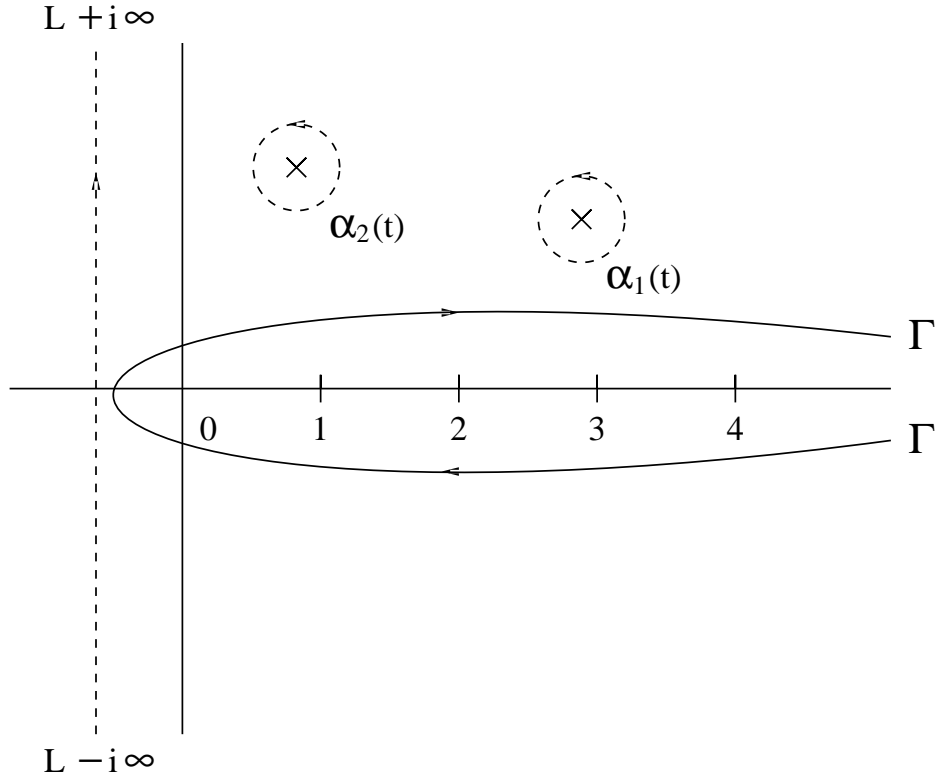


Figure 3: Various contours used for the Sommerfeld-Watson representation.

This naive expectation will be justified below even without this narrow-spread assumption. The function $\alpha(t)$ is known as a *Regge trajectory*.

Let us assume $a_\ell(t)$ to be an analytic function of ℓ , dying off sufficiently fast at infinity to enable the Sommerfeld-Watson representation to be used. We can then replace the sum (2.3) by a contour integral wrapping around the positive real ℓ -axis,

$$T(s, t) = -\frac{1}{2i} \int_{\Gamma} d\ell (2\ell + 1) a_\ell(t) \frac{P_\ell(-z_t)}{\sin \pi \ell}, \quad (2.4)$$

as shown in Fig. 3.

Suppose $a_\ell(t)$ has (Regge) poles located at $\ell = \alpha_i(t)$ with residue $\beta_i(t)/(2\alpha_i(t) + 1)$. Opening up the contour Γ and moving it to the left of the poles, we get

$$T(s, t) = -\frac{1}{2i} \int_{L-i\infty}^{L+i\infty} d\ell (2\ell + 1) a_\ell(t) \frac{P_\ell(-z_t)}{\sin \pi \ell} - \sum_i \frac{\pi \beta_i(t)}{\sin \pi \alpha_i(t)} P_{\alpha_i(t)}(-z_t), \quad (2.5)$$

where L is smaller than the real part of all $\alpha_i(t)$. The high-energy behavior is now dominated by the rightmost Regge pole $\alpha(t)$ to be

$$(-z_t)^{\alpha(t)} \simeq (2s/t)^{\alpha(t)}, \quad (2.6)$$

agreeing with the naive expectation.

In trying to get to this quickly I have glossed over a number of fine points. I have not discussed why $T(s, t)$ is analytic but that can be established at least in perturbation theory. I have ignored the spins of the colliding particles which complicate matter but pose no essential difficulty. Helicity is conserved at high energies and the dominant amplitude is helicity independent, so for elastic scattering everything is essentially the same as if the beam and target particles were without spin anyway. Another caveat is that the asymptotic behavior (2.2) is valid only when $\text{Re}(\ell) > -\frac{1}{2}$ so one might worry about the general validity of (2.6). It turns out that this can always be fixed up to render (2.6) valid.

I have also not discussed why it is reasonable to assume $a_\ell(t)$ to be analytic in ℓ . In fact, this is not even true unless the *signature* factor is taken into account.

To see what signature is let us suppose the particle A is its own antiparticle: $\bar{A} = A$. Then there is a forward-backward symmetry for the t channel process $\bar{B} + B \rightarrow \bar{A} + A$ so that the amplitude $T(s, t)$ is $s \leftrightarrow u$ symmetric. From (2.1) and (2.3), we see that only even angular momenta ℓ are present; $a_\ell(t)$ would be zero for odd ℓ . One would therefore expect that only even ℓ values are smoothly connected by the function $a_\ell(t)$.

This example suggests that we should always decompose an amplitude $T(s, t)$ into its $s \leftrightarrow u$ symmetric/antisymmetric parts $T_\pm(s, t)$. Both $a_\pm(t)$ are analytic but they may have different singularities, so the Regge trajectories for these two will generally be different. These two kinds of Regge trajectories are said to have even/odd signatures. When we replace T in (2.3) by T_\pm , the right-hand side should be replaced by $P_\ell(z_t) \pm P_\ell(-z_t)$, so the last factor in (2.5) and (2.6) become

$$\begin{aligned} \frac{1}{\sin \pi \alpha_i(t)} [P_{\alpha_i(t)}(-z_t) \pm P_{\alpha_i(t)}(z_t)] &\rightarrow \frac{1}{\sin \pi \alpha_i(t)} [(-z_t)^{\alpha_i(t)} \pm (z_t)^{\alpha_i(t)}] \\ &\rightarrow \left(\frac{s}{t}\right)^{\alpha_i(t)} \frac{1}{\sin \pi \alpha_i(t)} [1 \pm e^{\pi i \alpha_i(t)}]. \end{aligned} \quad (2.7)$$

The factor $(1 \pm e^{\pi i \alpha(t)})/\sin \pi \alpha(t)$ blows up at even/odd integer angular momenta J . This pole at $t = m_J^2$ corresponds to a resonance in the t -channel with mass m_J and spin J , so the Regge trajectory $\alpha(t)$ may be regarded as a trajectory connecting particles in the $J - m_J$ plane. Extrapolating this trajectory to negative t , it will determine the high-energy behavior of the s -channel amplitude, and this is the power of the Regge theory! However, this would work only if the singularities of $\alpha_\ell(t)$ in ℓ are indeed poles, an assumption that requires explicit verification and is not automatically guaranteed. In fact, as we shall see, the pole assumption appears to be true for the gluon trajectory but not the Pomeron trajectory that is discussed see below. Experimentally the total cross-section grows with energy, thus from (1.7) and (2.7) it follows that the leading regge intercept is at least 1, $\alpha(0) \geq 1$. However, the Froissart bound forbids the total cross-section to grow faster than $(\ln s)^2$ asymptotically, so this leading singularity, called the *Pomeron* trajectory or the *Pomeron* for short, must have a unit intercept $\alpha(0) = 1$, but then it cannot be a simple pole for otherwise the total cross-section would be a constant. It may be a double pole or

something more complicated. The usual view is that in QCD it is a composite object made up of two and more reggeized gluons.

2.2 QED to $O(g^6)$

Let us now turn to actual calculations of high energy processes in QED. We will follow the book of Cheng and Wu [6] from which one can find more details, as well as references to the original literature. We will concentrate specifically on electron-electron elastic scattering in the following.

The incoming beams will be assumed to move in the z -direction. At high energy it is convenient to use the lightcone coordinates $a_{\pm} = a^0 \pm a^3$, in terms of which the dot product of two four-vectors $a = (a_+, a_-, a_{\perp})$ and $b = (b_+, b_-, b_{\perp})$ is given by $ab = \frac{1}{2}(a_+b_- + a_-b_+) - a_{\perp} \cdot b_{\perp}$. The momenta of the incoming beams in the CM system are $p_1 = (\sqrt{s}, 0, 0)$ and $p_2 = (0, \sqrt{s}, 0)$, with masses ignored. We will make it a practice to draw p_1 on top and p_2 at the bottom in all the scattering diagrams.

We shall label the loop momenta by q_i and define the scaled ‘-’ momenta to be $x_i = q_{i-}/\sqrt{s}$. The measure for loop integration in lightcone variables is

$$\begin{aligned} \frac{i}{(2\pi)^4} d^4q &= \frac{i}{8\pi^2} dq_+ dq_- \frac{1}{(2\pi)^2} d^2q_{\perp} = \frac{1}{4\pi} \left[\frac{\sqrt{s}}{-2\pi i} dq_+ \right] dx \left[\frac{1}{(2\pi)^2} d^2q_{\perp} \right] \\ &\equiv \frac{1}{4\pi} [Dq_+] dx [Dq_{\perp}] . \end{aligned} \quad (2.8)$$

The momenta along the upper electron line are $p_1 + Q$, with Q being some combination of q_i (see Figs. 4 and 5 for illustrations). In the leading-log approximation when $|\Delta| = \sqrt{-t}$ is fixed and $s \rightarrow \infty$, we can approximate the electron propagator by

$$\frac{M + \gamma(p_1 + Q)}{(p_1 + Q)^2 - M^2 + i\epsilon} \simeq \frac{M + \gamma p_1}{2p_1 \cdot Q + i\epsilon} . \quad (2.9)$$

Since

$$M + \gamma p_1 = \sum_{\lambda} u_{\lambda}(p_1) \bar{u}_{\lambda}(p_1) , \quad \bar{u}_{\lambda'}(p_1) \gamma^{\mu} u_{\lambda}(p_1) = (2p_1^{\mu}) \delta_{\lambda'\lambda} , \quad (2.10)$$

we may simply drop all the γ matrices and spinor numerators, and consider the vertices to be $2p_1^{\mu}$. The same is true for the lower electron line where vertices can be taken to be $2p_2^{\mu}$. Physically, this expresses the simple fact that the large electric current carried by an electron at high energy is a result of its fast motion, with its magnetic moment contributing only a negligible amount. For the same reason the current of a spin-1 particle can be taken to be $2p^{\mu}$, which is valid even when that is the color current imbedded in a triple-gluon vertex in QCD, because the other two terms in the vertex are of order Δ/\sqrt{s} and can be neglected.

The procedure to follow to compute the high-energy amplitude is as follows:

1. Use residue calculus and flow diagrams to compute the ‘+’ integration.
2. Then obtain powers of $(\ln s)$ from the ‘-’ integrations.
3. The $q_{i\perp}$ integrations are never explicitly carried out.

2.2.1 The ‘+’ integration

Let us consider step 1 in more detail.

First of all, $a \cdot b$ is linear in a_+ and b_+ , hence the denominators of all propagators are linear in q_{i+} . This then provides one simple pole per propagator for the ‘+’ integrations. The integration contour is originally along the real q_{i+} axis, but we will close it with an extra half circle on the upper plane or the lower plane. By using $-q_{i+}$ as the integration variable if necessary, we can and will always choose to close the contour in the lower plane. The result of the integral is therefore equal to $-2\pi i$ times the residue at the pole, summed over all poles in the lower plane. The important question to decide then is which are the poles in the lower plane, and which are the poles in the upper plane. This clearly depends on the sign of the ‘-’ components, but they are integration variables and hence vary. The *flow diagrams* are invented to get the various possibilities sorted out [6].

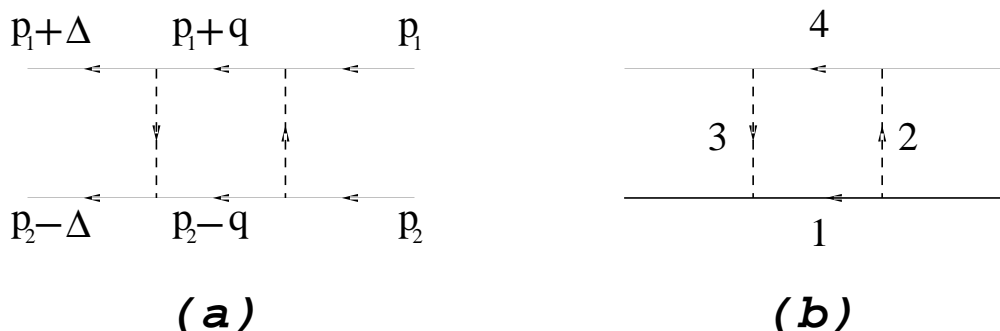


Figure 4: A one-loop Feynman diagram (a) and its flow diagram (b).

Figs. 4(a) and 5(a) are Feynman diagrams and 4(b), 5(b), and 5(c) are flow diagrams. The latter are diagrams indicating flows of the ‘-’ components of the momenta, subject to momentum conservation at each vertex. Arrows going one way (clockwise or counter clockwise) correspond to positive ‘-’ components, and arrows going the other way correspond to negative ‘-’ components. Which is which does not matter because we can always change the integration variable from q_{i+} to $-q_{i+}$ to compensate our choice.

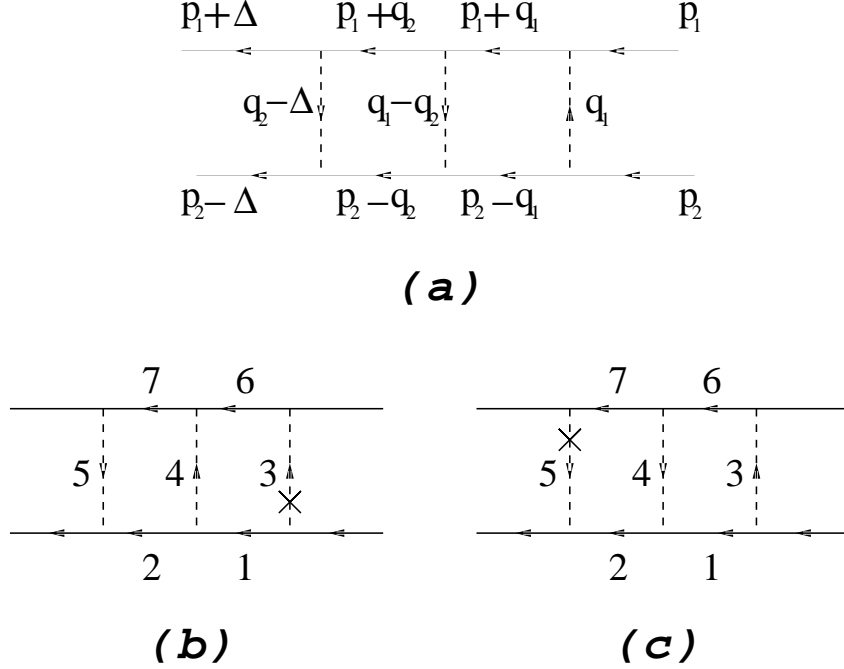


Figure 5: A two-loop Feynman diagram (a) and its flow diagrams (b) and (c).

Note that we have not included in Figs. 4 and 5 any flow diagram in which the arrows go around in the same direction in a close loop, for this gives rise to poles all in the same half plane so the ‘+’ integration would vanish. In making up flow diagrams, such closed loops are always excluded. In particular, this means that at the injection vertex where p_2 enters, and at the ejection vertex where p_2' leaves, the arrows are always arranged in the way shown in these diagrams. This rule determines uniquely the flow pattern of a one-loop diagram, as shown in 4(b), but it does not do so for diagrams of two or more loops, as the flow direction at the boundary of two loops can always be reversed. For two loops we have two flow diagrams, 5(b) and 5(c), and for more loops there are more flow diagrams.

Since we would like to have as few poles as possible in the lower plane, we would choose those directions in every loop with less arrows to correspond to poles in the lower plane. These are indicated by a cross (x) in the flow diagrams.

In the case of the right-hand loop in 5(b), there are two arrows along each direction, so it would seem to have two equally valid choices of poles for the lower plane. However, the ones indicated are preferred for two reasons.

First and foremost, it is never a good idea to choose a pole at the boundary of two loops. A pole within loop i determines the value of q_{i+} by the location of the pole, but a pole at the boundary of loops i and j determines only the combination $q_{i+} + q_{j+}$ which is less convenient.

There is a second reason for that choice. With the approximation (2.9), q_{i+} never appears on a propagator along the top line, so apparent poles there are actually absent. With that, the choice indicated actually has only one pole per loop.

2.2.2 The ‘-’ integration

The inverse propagators along the upper electron line is given by (2.9) to be sX , where $X = Q_-/\sqrt{s}$ is some linear combination of x_i , and each x_i in a flow diagram is by definition positive. The $\ln s$ factors are typically obtained from $\int_\epsilon dx_i/x_i$, where $\epsilon \sim \Delta^2/s$ represents a cutoff of x_i above which the approximation (2.9) is valid. For that reason, we can usually ignore all x_i compared to 1 in the leading-log approximation.

To proceed further it is convenient to adopt some shorthand notations. We will write $a_m = k_{m\perp}^2$ if k_m is the four-momentum of the m th line. If its pole is in the upper plane, we let d_m^{-1} to be its propagator. If it is in the lower plane, we let d_m^{-1} to be its residue multiplied by \sqrt{s} . It is understood that all of them are evaluated at the lower-plane pole positions, and the minus sign in the gluon propagator is included in this factor.

From (2.8), we see that the T-matrix after the Dq_{i+} integrations is given by the formula

$$T = - \int \left[\prod_{i=1}^{\ell} \frac{dx_i}{4\pi} Dq_{i\perp} \right] \frac{N}{D} . \quad (2.11)$$

Here ℓ is the number of loops in the diagram, $D = \prod_m d_m$, and N is the numerator factor coming from products of vertex factors. The lower limits of x_i can be taken to be $\epsilon = \Delta^2/s$. The minus sign comes from the overall sign factor in the last item of Sec. 1.3.

2.2.3 Fig. 4

From Figs. 4(a) and 4(b), we see that the pole is located at $q_+ = a_1/(1-x)\sqrt{s} \simeq a_1/\sqrt{s}$, with $d_1 = (1-x) \simeq 1$. The rest of the d -factors are $d_2 = a_2, d_3 = a_3, d_4 = sx$, so $D \simeq 1 \cdot a_2 \cdot a_3 \cdot sx$. The numerator is $N = g^4[(2p_1) \cdot (2p_2)]^2 = g^4(4s^2)$, so the T-matrix of this diagram is obtained from (2.11) to be

$$\begin{aligned} T &= -\frac{g^4 s}{\pi} \int Dq_{\perp} \frac{1}{a_2 a_3} \int_{\Delta^2/s} \frac{dx}{x} \\ &= -\frac{s}{\pi} (\ln s) g^2 I_2(\Delta) , \end{aligned} \quad (2.12)$$

where

$$I_n(\Delta) = \int \left[\prod_{i=1}^n \frac{d^2 q_{i\perp}}{(2\pi)^2} \right] (2\pi)^2 \delta\left(\sum_{i=1}^n q_{i\perp} - \Delta\right) . \quad (2.13)$$

In terms of convolution defined by

$$(F * G)(\Delta) \equiv \int \frac{d^2 q_{\perp}}{(2\pi)^2} F(\Delta - q_{\perp}) G(q_{\perp}) , \quad (2.14)$$

the function I_n is the n th-power convolution of I_1 with itself, which we write as

$$I_n(\Delta) = (*I_1)^n(\Delta) . \quad (2.15)$$

The impact-parameter-space function $\tilde{F}(b)$ is the Fourier transform of $F(q_\perp)$,

$$\tilde{F}(b) \equiv \int \frac{d^2 q_\perp}{(2\pi)^2} F(q_\perp) \exp(-iq_\perp \cdot b) . \quad (2.16)$$

Such functions are convenient because in this space convolutions turn into ordinary products in the usual way: $[F \widetilde{*} G](b) = \tilde{F}(b)\tilde{G}(b)$. Hence $\tilde{I}_n(b) = [I_1(b)]^n$.

2.2.4 Fig. 5

First consider flow diagram 5(b). The poles are located at $q_{2+} = a_2/(1-x_2)\sqrt{s} \simeq a_2/\sqrt{s}$, with $d_2 \simeq 1$, and $q_{1+} = a_3/x_1\sqrt{s}$ with $d_3 = x_1$. The rest of the d -factors are $d_1 = (p_2 - q_1)_+(p_2 - q_1)_- - a_1 \simeq -a_3/x_1 - a_1 \simeq -a_3/x_1$, $d_4 = -(q_1 - q_2)_+(q_1 - q_2)_- + a_4 \simeq -(x_1 - x_2)a_3/x_1 + a_4$, $d_5 = a_5$, $d_6 = sx_2$, $d_7 = sx_1$. Hence $D = 1 \cdot (-a_3/x_1) \cdot a_3 \cdot \{[x_2 a_3 + x_1(a_4 - a_3)]/x_1\} \cdot x_1 \cdot sx_2 \cdot sx_1 \simeq -s^2 x_2 a_3 a_5 [x_2 a_3 + x_1(a_4 - a_3)]$. The numerator is $N = g^6 (2s)^3$, so the contribution from 5(b) is

$$\begin{aligned} T_b &= \frac{g^6 s}{2\pi^2} \int Dq_{1\perp} Dq_{2\perp} \frac{1}{a_3 a_5} \int \frac{dx_1 dx_2}{x_2 [x_2 a_3 + x_1 (a_4 - a_3)]} \\ &= \frac{g^6 s \ln s}{2\pi^2} \int Dq_{1\perp} Dq_{2\perp} \frac{\ln(a_4/a_3)}{a_3 a_5 (a_4 - a_3)} . \end{aligned} \quad (2.17)$$

The flow diagram 5(c) gives identical result so the total is

$$\begin{aligned} T &= T_b + T_c = -\frac{s \ln s}{\pi^2} g^6 J_3(\Delta) , \\ J_3(\Delta) &\equiv \int Dq_{1\perp} Dq_{2\perp} \frac{\ln(a_4/a_3)}{a_3 a_5 (a_4 - a_3)} . \end{aligned} \quad (2.18)$$

2.2.5 2nd, 4th, and 6th order QED diagrams

QCD diagrams up to $O(g^6)$ are shown in Fig. 6, but for now we are interested only in those that contribute to QED electron scatterings. These are diagrams A, B1, B2, C15–C20.

B1 and C15 were computed above, others can all be computed in a similar manner. The contribution to $T/(2s)$ from each diagram is [6]:

$$\begin{aligned} A &= -g^2 I_1 \\ B1 &= -\frac{\ln(se^{-\pi i})}{2\pi} g^4 I_2 \\ B2 &= +\frac{(\ln s)}{2\pi} g^4 I_2 \\ C15 &= -\frac{(\ln s)}{2\pi^2} g^6 J_3 \end{aligned}$$

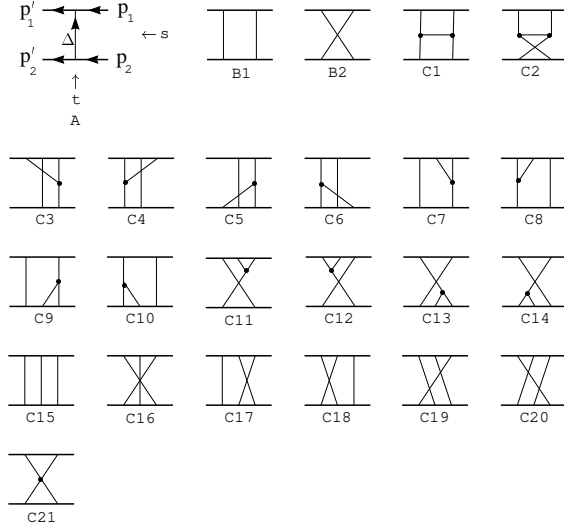


Figure 6: QCD scattering diagrams to $O(g^6)$. The QED diagrams come from the following subset: A, B1, B2, and C15 to C20.

$$\begin{aligned}
C16 &= -\frac{(\ln s)}{2\pi^2} g^6 J_3 \\
C17 &= +\frac{(\ln s)}{4\pi^2} g^6 (J_3 + \pi i I_3) = C18 \\
C19 &= +\frac{(\ln s)}{4\pi^2} g^6 (J_3 - \pi i I_3) = C20 .
\end{aligned} \tag{2.19}$$

The total contribution up to $O(g^6)$ is obtained by adding up all the expressions in (2.19). The interesting, but sad thing, is that the $(\ln s)$ contributions all add up to cancel one another. It turns out that the $O(1)$ contribution from $B1 + B2$ is shown correctly in (2.19), but that of the sum of C15 to C20 is not. So in order to get a nonzero sum for those a much more difficult calculation accurate to $O(1)$ would have to be carried out.

3 ABELIAN CUT DIAGRAMS

3.1 Factorization Formula

We want to deal with tree diagrams like Fig. 7, in which the momentum p is much larger than all the momenta q_i , so that the following approximation for the denominator of propagators is valid:

$$\left(p + \sum_{j=1}^i q_j\right)^2 - m^2 \simeq 2p \cdot \sum_{j=1}^i q_j \equiv \sum_{j=1}^i \omega_j \tag{3.1}$$

This is the same approximation used earlier in (2.9).

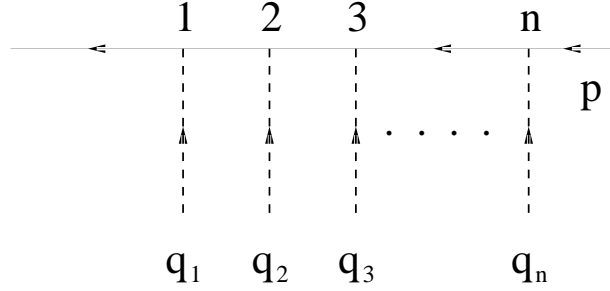


Figure 7: A tree diagram, to be designated by the order of the dotted lines from left to right, as $[12 \cdots n]$.

A tree will be denoted according to the ordering of lines q_i , so the one shown in Fig. 7 is then $[12 \cdots n]$. Its scalar tree amplitude is

$$a[12 \cdots n] = -2\pi i \delta\left(\sum_{j=1}^n \omega_j\right) \left(\prod_{i=1}^{n-1} \frac{1}{\sum_{j=1}^i \omega_j + i\epsilon} \right). \quad (3.2)$$

In this subsection we will show that certain sums of amplitudes of this type can be expressed as a factorized product.

We need some notations. If $[T_i]$ are tree diagrams, then $[T_1 T_2 \cdots T_A]$ is the tree diagram obtained by merging these A trees together. For example, if $[T_1] = [123]$ and $[T_2] = [45]$, then $[T_1 T_2] = [12345]$. The notation $\{T_1; T_2; \cdots; T_A\}$, on the other hand, is used to denote the *set* of all tree diagrams obtained by *interleaving* the trees T_1, T_2, \cdots, T_A in all possible ways. This set contains $(\sum_a n_a)! / \prod_a n_a!$ trees if n_a is the number of gluon lines in the tree T_a . In the example above, $\{T_1; T_2\}$ contains the following $5!/3!2! = 10$ trees: $[12345]$, $[12435]$, $[12453]$, $[14235]$, $[14253]$, $[14523]$, $[41235]$, $[41253]$, $[41523]$, and $[45123]$.

Correspondingly, $a\{T_1; T_2; \cdots; T_k\}$ will represent the sum of the amplitudes $a[T]$ for every tree T in this set. The *factorization formula* [1] states that this sum can be factorized into a product:

$$a\{T_1; T_2; \cdots; T_A\} = \prod_{a=1}^A a[T_a] \equiv a[T_1 | T_2 | \cdots | T_A]. \quad (3.3)$$

Proof: Let $[T] = [t_1 t_2 \cdots t_n]$ be a tree and $a[T]$ its scalar amplitude defined by (3.2). Then

$$\begin{aligned} a[T] &= (-i)^n \int_{T_o} d^n \tau \exp\left(i \sum_{i=1}^n \omega_{t_i} \tau_{t_i}\right) \\ \int_{T_o} d^n \tau &\equiv \int_{-\infty}^{\infty} d\tau_{t_n} \int_{\tau_{t_n}}^{\infty} d\tau_{t_{n-1}} \cdots \int_{\tau_{t_2}}^{\infty} d\tau_{t_1}, \end{aligned} \quad (3.4)$$

where the integration region T_o is defined by the ordering $\infty > \tau_{t_1} \geq \tau_{t_2} \geq \cdots \geq \tau_{t_n} > -\infty$. When summed over all $T \in \{T_1; T_2; \cdots\}$, the integration variables τ_{t_a} retains only the

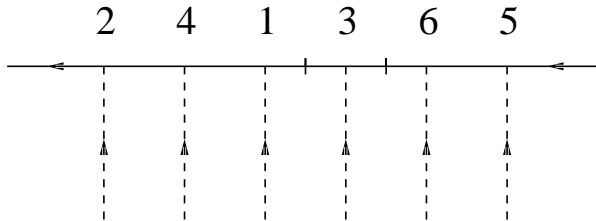


Figure 8: The abelian cut diagram $[241|3|65]$.

ordering within each individual tree T_i , and for each tree they integrate from $-\infty$ to $+\infty$. Using (3.4) again for individual trees T_i , we obtain (3.3). (*end of proof*)

There is a close affinity between the factorization formula and the string-like representation. See Ref. [12] for a discussion on this point.

The right-hand-side of (3.3) can be regarded as the amplitude $a[T_1|T_2|\cdots|T_A]$ of the *cut diagram* $[T_1|T_2|\cdots|T_A]$. This is just the diagram $[T_1T_2\cdots T_A]$ with cuts put on the propagators right after $T_1, T_2, \cdots, T_{A-1}$. The *cut amplitude* $a[T_1|T_2|\cdots|T_A]$ is obtained from $a[T_1T_2\cdots T_A]$ by using the Cutkosky propagator $-2\pi i\delta(\sum_j \omega_j)$ on the cut lines instead of the Feynman propagator $(\sum_j \omega_j + i\epsilon)^{-1}$.

For example, the cut diagram $[241|3|65]$ is shown in Fig. 8 and the corresponding cut amplitude is $a[241|3|65] = a[241]a[3]a[65]$. Note that the sections between cuts in a cut amplitude can be permuted at will, so for example, $a[241|3|65] = a[3|65|241]$. We shall refer to this as the *commutative property* of the abelian cut amplitude.

The factorization formula can be used to sum up *loop* amplitudes as well. This is because (3.3) is valid whether q_i are onshell or not, so the tree in Fig. 7 or 8 may very well be just a section of a much larger loop diagram, in which case (3.3) gives a sum of loop diagrams in terms of a single cut diagram. We shall call these *abelian cut diagrams*.

Abelian cut diagrams resemble Cutkosky cut diagrams but they are quite different. Cuts here are only put on a high-momentum tree, and the resulting cut diagram represents a summation of Feynman diagrams rather than the discontinuity of one of them.

In the simple case when every tree $[T_i] = [i]$ is a vertex containing a single line, the factorization formula can be written as

$$a[1; 2; \cdots; A] = a[1|2|\cdots|A] . \quad (3.5)$$

This is called the *eikonal formula* and it has been known for a long time [7].

A single abelian cut diagram represents a sum of Feynman diagrams, nevertheless it is easier to evaluate a single cut diagram than even a single Feynman diagram. This is mainly because there are fewer flow diagrams present in a cut diagram than a Feynman diagram. To

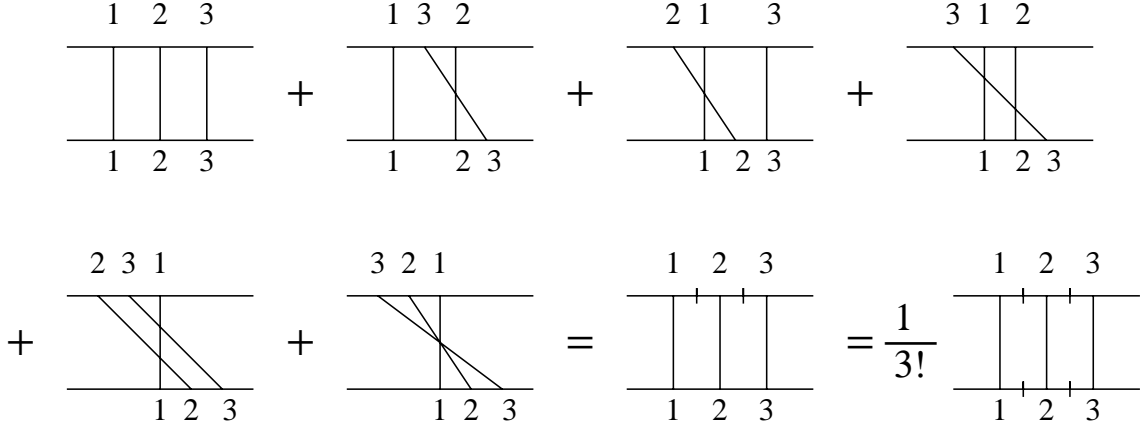


Figure 9: The six s -channel-ladder diagrams for $n = 3$.

see that, suppose cuts are made on the tree of the top line, which is what we will usually do. A cut propagator is given by $-2\pi i\delta(sX)$ (see Sec. 2.2.2 for notation). Now $\sqrt{s}X$ is the ‘-’ flow through the line, which must now be zero because of the presence of the δ -function, so a cut propagator is ‘cut’ also in the sense of severing the flow. This limits the various ways the ‘-’ flow can go around the diagram and hence the number of possible flow diagrams.

3.2 The Sum of QED s -Channel-Ladder Diagrams

A $(2n)$ th order s -channel-ladder diagram for electron-electron scattering is obtained by tying together the n photons from two electron trees like Fig. 7. There are all together $n!$ diagrams of this type depending on how the lines from the two trees are tied. Fig. 9 shows the 6 diagrams for the case $n = 3$.

These $n!$ diagrams can be labelled by the order of the photons $[\sigma_1\sigma_2\cdots\sigma_n]$ on the upper tree, when their order on the lower tree is fixed to be $[12\cdots n]$.

Use (3.5) to sum over the $n!$ permuted upper trees, the result is an upper tree with all its propagators cut, as shown in the diagram between the two equal signs in Fig. 9 for the case $n = 3$. We may now use the commutative property of an abelian cut amplitude to symmetrize the photon lines attached to the *lower tree*. Use (3.5) again but now on the lower tree, we get a double-cut planar diagram, where all the electron propagators on the upper and on the lower trees are cut. A factor $n!$ is needed to convert the symmetrization into addition. For $n = 3$ this is shown in the last diagram of Fig. 9.

The double-cut diagram is now easy to compute and one gets

$$\frac{T_n}{2s} = -\frac{1}{n!} \int \left[\prod_{i=1}^{n-1} (2s)g^2 Dq_{i\perp} \frac{1}{a_i} \frac{i}{8\pi^2} dq_{i+} dq_{i-} (-2\pi i)^2 \delta(\sqrt{s}q_{i+}) \delta(\sqrt{s}q_{i-}) \right] \frac{g^2}{a_n}$$

$$= -\frac{g^{2n}}{n!}(-i)^{n-1}I_n(\Delta) , \quad (3.6)$$

where I_n is defined in (2.13) and (2.15).

Let us compare the result with those obtained in (2.19) by direct calculations. For $n = 1$, this should equal to A of (2.19) and indeed it does. For $n = 2$, it should be $B1 + B2$ and again it is. Note that individually $B1$ and $B2$ are of order $\ln s$. To compute the sum which is of $O(1)$ correctly we need to know each *Feynman diagram* to subleading-log accuracy. A *cut diagram* is already a sum so each can be computed just in the leading-log approximation as was done in (3.6). This ability to avoid subleading-log calculation is the main advantage of the cut diagrams.

This is further illustrated by looking at $n = 3$, whose correct result is shown in (3.6) to be $g^6 I_3/3!$. This cannot even be obtained from (2.19) because the calculation of order g^6 there is accurate only to leading log.

In the impact-parameter space, (3.6) is given by

$$\frac{\tilde{T}_n(b)}{2s} = -i\frac{1}{n!}[-ig^2\tilde{I}_1(b)]^n . \quad (3.7)$$

Summing over all n , we get an impact-parameter representation of the T -matrix in the eikonal form:

$$\begin{aligned} \frac{T}{2s} &= \sum_{n=1}^{\infty} \int d^2b \exp(iq_{\perp} \cdot b) \frac{\tilde{T}_n(b)}{2s} \\ &= -i \int d^2b e^{iq_{\perp} \cdot b} \{ \exp[-ig^2\tilde{I}_1(b)] - 1 \} . \end{aligned} \quad (3.8)$$

This elegant expression has been known for a long time [6]. It is call the eikonal formula for high-energy scattering and is where the ‘eikonal formula’ (3.5) derived its name from. This S -matrix is unitary, with $-g^2\tilde{I}_1(b)$ being essentially the phase shift an electron accumulated when it shoots by another electron at an impact parameter b . High energy approximation enters by assuming the electrons travel essentially at a straight-line trajectory with fixed impact parameter (perpendicular distance between the scattered electrons) fixed. It leads to a total cross-section independent of energy. If pair productions in the intermediate states are included, then a rising total cross-section can be obtained [6].

3.3 Other Sum Rules for QED

In the last subsection we illustrated the power of the eikonal formula (3.5) in computing sums of all ladder diagrams. We shall give two examples in this subsection to illustrate the more general factorization formula (3.3) in computing other sums. These two examples are shown in Figs. 10 and 11.

In each case, (3.3) is applied to the upper tree with the lower tree held fixed. The two cases correspond respectively to the identities

$$a\{31; 2\} = a\{31|2\} \quad (3.9)$$

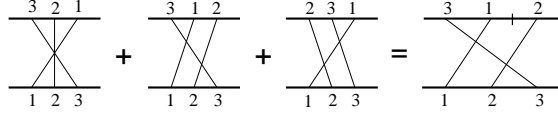


Figure 10: An example of using the factorization formula (3.3) to convert a sum of Feynman diagrams into a single abelian cut diagram.

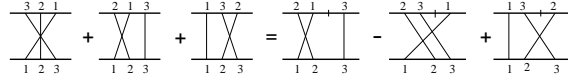


Figure 11: Another example of using the factorization formula (3.3) to convert a sum of Feynman diagrams into a sum of abelian cut diagrams.

$$\begin{aligned}
 a[321] + a[231] + a[132] &= a\{21; 3\} - a\{23; 1\} + a\{13; 2\} \\
 &= a[21|3] - a[23|1] + a[13|2] .
 \end{aligned} \tag{3.10}$$

We shall now compute the abelian cut diagrams and compare them with the result obtained by computing Feynman diagrams.

The flow diagrams for the four abelian cut diagrams are shown in Fig. 12. The flow in each case is unique, and the two poles for the two ‘+’ integrations can all be taken at the bottom electron line. The computation is as before, and the result for Figs. 12 (a),(b),(c),(d) are respectively

$$\begin{aligned}
 T_a &= -g^6(2s)(-i)\frac{1}{2\pi}(-\ln s)I_3(\Delta) = -T_d \\
 T_b &= T_c = 0 .
 \end{aligned} \tag{3.11}$$

The reason for the second equation is because in both 12(c) and 12(d) the arrows in one of the two loops are all in the same directions.

The sum rules displayed in (3.9), (3.10), Fig. 10, and Fig. 11 demand that

$$C16 + C19 + C20 = \frac{T_a}{2s} \tag{3.12}$$

$$C16 + C18 + C17 = \frac{1}{2s}(T_b - T_c + T_d) , \tag{3.13}$$

which can be seen to be true from (2.19), (3.12), and (3.13).

In these two sum rules the leading $\ln s$ is not cancelled, but the complicated transverse function J_3 in (2.19) is.

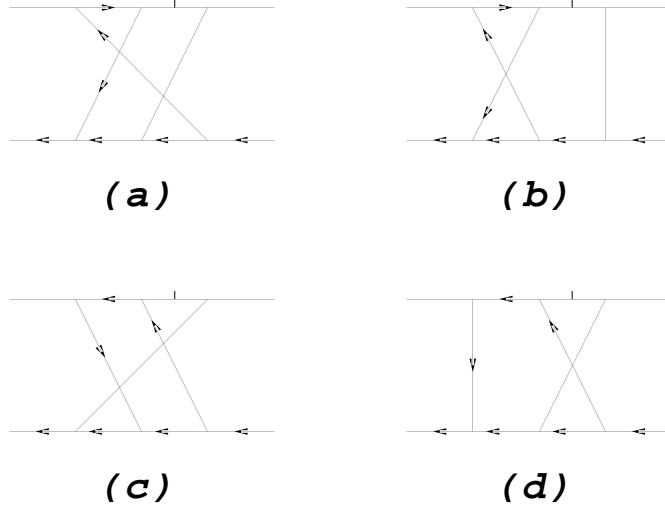


Figure 12: Flow diagrams to compute the right-hand-side of eq. (3.9) (diagram (a)) and eq. (3.10) (diagrams (b),(c),(d)).

4 NONABELIAN CUT DIAGRAMS

4.1 Multiple Commutator Formula

In this section we consider the generalization of the eikonal formula (3.5) to nonabelian amplitudes. In other words, given a tree diagram (Fig. 7) with nonabelian vertices t_a and amplitude $a[12 \cdots n] \cdot t[12 \cdots n] \equiv a[12 \cdots n] \cdot t_1 t_2 \cdots t_n$, we wish to find an expression for the sum of the $n!$ permuted amplitudes to be expressed in terms of cut diagrams. This turns out to be the *multiple commutator formula* [1], which states that

$$\sum_{\sigma \in S_n} a[\sigma] t[\sigma] = \sum_{\sigma \in S_n} a[\sigma_c] t[\sigma'_c], \quad (4.1)$$

where $S_n = \{1; 2; \cdots; n\}$, $a[\sigma]_c$ is an abelian cut amplitude (see Sec. 3.1) for the cut diagram $[\sigma]_c$, and $t[\sigma'_c]$ is the corresponding nonabelian factor computed from the *complementary cut diagram* $[\sigma'_c]$.

The cut diagram $[\sigma]_c$ is obtained by putting cuts in the Feynman tree $[\sigma]$ in the following way. Proceeding from left to right, a cut is put after a number iff there is not a smaller number to its right. An external line is considered as a cut so there is never any need to have an explicit cut at the end of a tree.

Here are some examples of where cuts should be put: $[1234]_c = [1|2|3|4]$, $[3241]_c = [3241]$, and $[2134]_c = [21|3|4]$.

The *complementary cut diagram* $[\sigma'_c]$ is one where lines cut in $[\sigma_c]$ are not cut in $[\sigma'_c]$, and vice versa. Thus $[1234]'_c = [1234]$, $[3241]'_c = [3|2|4|1]$, and $[2134]'_c = [2|134]$.

The nonabelian factor $t[\sigma'_c]$ is obtained from $t[\sigma]$ by replacing the product of nonabelian matrices separated by cuts with their commutators. For example, $t[1234]'_c = t[1234] = t_1 t_2 t_3 t_4$, $t[3214]'_c = t[3|2|4|1] = [t_3, [t_2, [t_4, t_1]]]$, and $t[2134]'_c = t[2|134] = [t_2, t_1] t_3 t_4$.

Let me now illustrate this by writing down explicitly the multiple commutator formula for $n = 3$. In that case $S_3 = \{1; 2; 3\}$ contains 6 trees, and the right-hand side of (4.1) is given by

$$\begin{aligned} a[1|2|3]t[123] + a[1|32]t[13|2] + a[21|3]t[2|13] + a[231]t[2|3|1] \\ + a[31|2]t[3|12] + a[321]t[3|2|1] . \end{aligned} \quad (4.2)$$

As before, the trees in S_n can be imbedded in much bigger Feynman diagrams, in which case the right-hand side of (4.1) and the corresponding *nonabelian cut diagrams* can be used to sum up loop diagrams as well.

Application of this formula will be discussed in Secs. 5 and 6. Before doing that, we shall sketch the proof of (4.1) in the next subsection.

4.2 Folding Formula

The proof of the multiple commutator formula relies on another combinatorial formula which I call the *folding formula* [1]:

$$a[RoS] = \sum_{k=0}^N (-)^k a\{R; \tilde{\sigma}_{1,k}.o\} a[\sigma_{k+1,N}] \equiv \sum_{k=0}^N (-)^k a\{R; \tilde{\sigma}_{1,k}.o|\sigma_{k+1,N}\} . \quad (4.3)$$

Let me explain the notation and the meaning of this formula.

Consider the amplitude of a tree $[RoS]$, put together from a tree $[R]$, followed by a line $[o]$, and then followed by another tree $[S]$. The tree $[S]$ is assumed to have N lines, with $[\sigma_{1,k}]$ denoting its subtree formed from the first k lines, and $\sigma_{k+1,N}$ its subtree formed from the remaining $N - k$ lines. In other words, $[S] = [\sigma_{1,k}\sigma_{k+1,N}]$ for every k . The trees $\sigma_{1,0}$ and $\sigma_{N+1,N}$ are taken to be the null tree $[\emptyset]$. By definition, $a[\emptyset] = 1$. The notation $\tilde{\sigma}_{1,k}$ means the tree $\sigma_{1,k}$ read in the reverse order. For example, if $[S] = [14327856]$, then $\sigma_{1,3} = [143]$, $\sigma_{4,8} = [27856]$, and $\tilde{\sigma}_{1,3} = [341]$.

Let $[t]$ be a tree, with or without cuts. The symbol $\{T_1; T_2; \dots; T_A.t\}$ is taken to mean the set of trees $[Tt]$ for all $[T] \in \{T_1; T_2; \dots; T_A\}$, and $a\{T_1; T_2; \dots; T_A.t\}$ is the sum of these amplitudes $a[Tt]$.

The folding formula (4.3) shows how $a[RoS]$ can be expressed as sums of products of amplitudes with line ‘ o ’ moved to the end of the tree in each case. Alternatively the line ‘ o ’ is moved to a position just before a cut and by the commutative property of abelian cut amplitudes (see Sec. 3.1) this is just as good as moving it to the end.

This formula is called the ‘folding formula’, or the *cutting and folding formula*, because the right-hand side can be obtained from the left-hand side first by *cutting* off the tree $\sigma_{k+1,N}$ at the end of $[RoS]$, and then *folding* the remaining tree about the point o , as shown

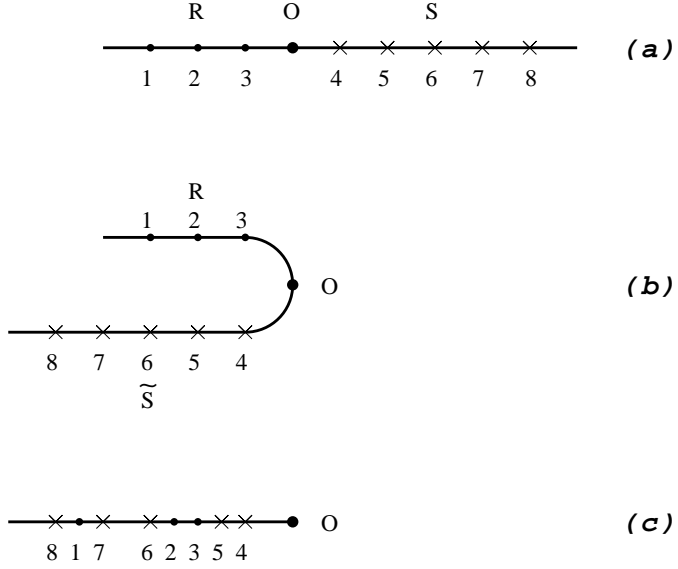


Figure 13: The folding formula illustrated. The cutoff part is not drawn.

in Fig. 13. Finally, both branches of the folded tree should be interleaved to obtain the trees $\{R; \tilde{\sigma}_{1,k}.o\}$ in (4.3).

The folding formula is proven from the factorization formula (3.3) by an inductive and combinatorial argument [1]. I shall not repeat the somewhat involved arguments here, but I will work out some simple cases to illustrate the formula and its proof.

Suppose we want to move line 1 of $a[2134]$ to the extreme right. Then in the notation of (4.3), we are faced with a situation where $[R] = [2]$, $[o] = [1]$, and $[S] = [34]$. Hence (4.3) gives

$$\begin{aligned}
 a[2134] &= a[21|34] - a\{2; 3.1\}a[4] + a\{2; 43.1\} \\
 &= a[21|34] - a[231|4] - a[321|4] + a[2431] + a[4231] + a[4321] . \quad (4.4)
 \end{aligned}$$

Let me now show you how the proof goes for simple cases. Suppose $[S] = [s]$ is a single line. Then (3.3) implies $a[Ro|s] = a\{Ro; s\} = a[Ros] + a[R; s.o]$, which leads immediately to the folding formula $a[Ros] = a[Ro|s] - a\{R; s.o\}$. If $[S] = [s_1s_2]$, then the proof goes in a similar way but is more involved. In that case we can use (3.3) to get $a[Ro|s_1s_2] = a\{Ro; s_1s_2\} = a[Ros_1s_2] + a\{R; s_1.os_2\} + a\{R; s_1s_2.o\}$. The term $a\{R; s_1.os_2\}$ can be computed from the $N = 1$ formula, which yields $a\{R; s_1.o\}a[s_2] - a\{R; s_1; s_2.o\}$. Substituting this back and noticing that

$$a\{R; s_1s_2.o\} - a\{R; s_1; s_2.o\} = -a\{R; s_2s_1.o\} , \quad (4.5)$$

we obtain the desired $N = 2$ result

$$a[Ros_1s_2] = a[Ro|s_1s_2] - a\{R; s_1.o\}a[s_2] + a\{R; s_2s_1.o\} . \quad (4.6)$$

Similar proof goes for any N .

I will now show how the multiple commutator formula (4.1) can be obtained from the folding formula (4.3).

Take any abelian Feynman amplitude $a[\sigma]$. Use (4.3) to cut and to fold, so as to move the number ‘1’ to the end. The result is a sum of product of two $a[\cdot\cdot\cdot]$, the first one having the number ‘1’ at the end, and the second one not containing the number ‘1’. Use (4.3) again to cut and to fold the second $a[\cdot\cdot\cdot]$, now to move the smallest number in its argument to the end, and so on. The final result is a complicated sum of products of several $a[\dots]$, each having the smallest number within its argument located at the end. In other words, each is a cut amplitude $a[\rho]_c$ of some cut diagram $[\rho]_c$ determined in the way specified in Sec. 4.1.

Conversely, given a $[\rho]_c$, we can obtain all the $[\sigma]$ ’s that gave rise to it this way by repeated unfoldings and gluings. To see how this works in more detail, let us first consider the case when $[\rho]_c$ contains no cut. That means the number ‘1’ is at the end, so it is of the form $[\rho]_c = [\tau 1]$. To unfold the tree $[\tau 1]$, pick out any two interleaving subsets $[\tau_1]$ and $[\tilde{\tau}_2]$ from $[\tau]$, in all possible ways, *viz.*, find all such τ_i so that $[\tau 1] \in \{\tau_1; \tilde{\tau}_2.1\}$. Then the desired trees after unfolding are $[\sigma] = [\tau_1 1 \tau_2]$. The sign involved in (4.3) is $(-)^k$, where k is the number of boson lines in tree $[\tau_2]$.

The nonabelian factors associated with $a[\sigma]$ is $t[\sigma]$, hence the nonabelian factor associated with $a[\rho]_c = a[\tau 1]$ is $\sum (-)^k t[\tau_1 1 \tau_2]$, which is nothing but the multiple commutator $t[\rho]'_c$.

We have now considered the case when $[\rho]_c$ has no explicit cuts. If $[\rho]_c$ has explicit cuts, then we can apply the argument above to each of the cut sections, to obtain a multiple commutator for the nonabelian factor of each cut section. Thus the nonabelian factor for $a[\rho]_c$ is always $t[\sigma]'_c$ as specified in Sec. 4.1, and the multiple commutator formula is proved. (*end of proof*)

5 QUARK-QUARK SCATTERING TO $O(g^6)$

5.1 Color Factors

The color factor of a quark-gluon vertex is t_a , and that for a triple gluon vertex is if_{abc} . Putting these together, and using (1.8) and (1.9), or graphically Fig. 1, the color factor for a QCD Feynman diagram can be computed [6]. In what follows we shall concentrate on ‘quark-quark’ scattering where the ‘quark’ is allowed to carry any color in an $SU(N_c)$ theory with any N_c . In other words, the ‘quarks’ below could very well have been gluons as far as color is concerned.

Fig. 14 contains an illustration as to how this can be done. For other examples see Ref. [6].

The color factor for a nonabelian cut diagram is computed in a similar way. Fig. 15 contains one such example.

To order $O(g^6)$, the color factors can all be reduced by this method to combinations of the four shown in Fig. 16 [2].

$$\begin{aligned}
\text{Diagram 1} &= \text{Diagram 2} - \text{Diagram 3} - \text{Diagram 4} \\
&= \text{Diagram 5} - \text{Diagram 6} + \text{Diagram 7} - \text{Diagram 8} \\
&= \text{Diagram 9} - \text{Diagram 10} - \text{Diagram 11} - \text{Diagram 12} \\
&= G_4 + 2cG_2 - G_3
\end{aligned}$$

Figure 14: An illustration for the computation of the color factor of a Feynman diagram

$$\begin{aligned}
\text{Diagram 1} &= -\text{Diagram 2} = -\text{Diagram 3} + \text{Diagram 4} \\
&= -c^2 \text{Diagram 5} - \text{Diagram 6} \\
&= -c^2 \text{Diagram 7} + \text{Diagram 8} = -c^2 \text{Diagram 9} + c^2 \text{Diagram 10} = 0
\end{aligned}$$

Figure 15: An illustration for the computation of the color factor of a nonabelian cut diagram.

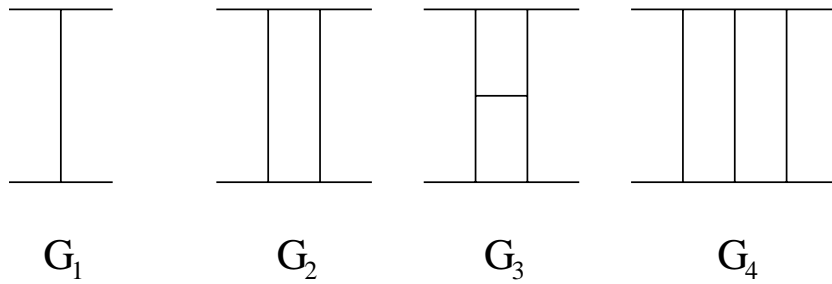


Figure 16: The four color factors for $O(g^6)$ diagrams.

5.2 Sum of Feynman Diagrams

To $O(g^6)$ the QCD Feynman diagrams for quark-quark scattering are shown in Fig. 6. Each of their color factors can be computed by the method of the last subsection, and each of its spacetime amplitude can be computed as in Sec. 2.2. In fact, those diagrams common to QED have already been listed already in (2.19). For others, see Ref. [6] for details of the computations.

Putting these together, The contribution from each diagram in Fig. 6 to $T/(2s)$ is ($\beta = g^2/2\pi$)

$$\begin{aligned}
A &= -g^2 I_1 \cdot \mathbf{G}_1 \\
B1 &= -g^2 \beta \ln(se^{-\pi i}) I_2 \cdot \mathbf{G}_2 \\
B2 &= +g^2 \beta (\ln s) I_2 \cdot (\mathbf{G}_2 + c\mathbf{G}_1) \\
\overline{C1} &= +g^2 \beta^2 \ln^2(se^{-\pi i}) \left[\frac{1}{2} \Delta^2 I_2^2 - J_2 I_2 \right] \cdot \mathbf{G}_3 \\
\overline{C2} &= -g^2 \beta^2 (\ln^2 s) \left[\frac{1}{2} \Delta^2 I_2^2 - J_2 I_2 \right] \cdot (\mathbf{G}_3 + c^2 \mathbf{G}_1) \\
C3 &= +g^2 \beta^2 \{ \ln^2(se^{-\pi i}) - \ln^2 s \} \frac{1}{4} J_2 I_2 \cdot (\mathbf{G}_3 - c\mathbf{G}_2) = C4 = C5 = C6 \\
C7 &= -g^2 \beta^2 \ln^2(se^{-\pi i}) \frac{1}{4} J_2 I_2 \cdot (-c\mathbf{G}_2) = C8 = C9 = C10 \\
C11 &= +g^2 \beta^2 (\ln^2 s) \frac{1}{4} J_2 I_2 \cdot (-c\mathbf{G}_2 - c^2 \mathbf{G}_1) = C12 = C13 = C14 \\
C15 &= -g^2 \beta^2 (\ln s) 2J_3 \cdot \mathbf{G}_4 \\
C16 &= -g^2 \beta^2 (\ln s) 2J_3 \cdot (\mathbf{G}_4 - \mathbf{G}_3 + 3c\mathbf{G}_2 + c^2 \mathbf{G}_1) \\
C17 &= +g^2 \beta^2 (\ln s) (J_3 + \pi i I_3) \cdot (\mathbf{G}_4 + c\mathbf{G}_2) = C18 \\
C19 &= +g^2 \beta^2 (\ln s) (J_3 - \pi i I_3) \cdot (\mathbf{G}_4 - \mathbf{G}_3 + 2c\mathbf{G}_2) = C20
\end{aligned} \tag{5.1}$$

The functions J_3 and I_n were already given in (2.21) and (2.16). The function J_2 is

$$J_2(\Delta) = \int \frac{d^2 q_\perp}{(2\pi)^2} \frac{1}{q_\perp^2} . \tag{5.2}$$

The sum of these diagrams is

$$\begin{aligned}
\frac{1}{2s} T &= -g^2 I_1 \left[1 - \bar{\alpha} \ln s + \frac{1}{2!} \bar{\alpha}^2 \ln^2 s \right] \cdot \mathbf{G}_1 + \frac{i}{2} (g^4 I_2 - \frac{c}{\pi} g^6 I_3 \ln s) \cdot \mathbf{G}_2 \\
&+ \frac{i}{2\pi} \ln s \left[g^6 I_3 - \frac{1}{2} g^6 \Delta^2 I_2^2 \right] \cdot \mathbf{G}_3 + \frac{1}{3!} g^6 I_3 \cdot \mathbf{G}_4 ,
\end{aligned} \tag{5.3}$$

where

$$\bar{\alpha}(\Delta) \equiv \frac{c}{2\pi} g^2 \Delta^2 I_2(\Delta) . \tag{5.4}$$

There are several things worth noting:

1. In the fourth order, the leading term proportional to $(\ln s)$ is cancelled out between $B1$ and $B2$ in the color amplitude \mathbf{G}_2 , though not in \mathbf{G}_1 .
2. In the sixth order, the leading $(\ln s)$ contributions to \mathbf{G}_4 from $C15$ to $C20$ also add up to zero. The expressions given in (5.1) are not accurate enough to deal with the subleading terms as already noted in Sec. 3.2. The term in (5.3) proportional to \mathbf{G}_4 is obtained separately from the eikonal formula.
3. *As a result of these cancellations*, the coupling-constant and energy dependences of the \mathbf{G}_i amplitude is of the form $g^{2m}(g^2 \ln s)^p$, where $m = 1, 2, 2, 3$ respectively for the color factors $i = 1, 2, 3, 4$, and p is determined by the order of the perturbation. Referring to Fig. 16, we see that m is simply the number of vertical lines in the color factor, or as we shall see in the next section, the number of reggeons being exchanged. It is important to note that this dependence is not true for individual Feynman diagrams.
4. To leading-log accuracy, the functions J_2 and J_3 get cancelled out. Only I_n appears in the final result.
5. The quantity in the square bracket in the \mathbf{G}_1 term of (5.3) is simply the the first three terms in the expansion of $\exp(-\bar{\alpha} \ln s)$. If we define the (transverse) reggeon propagator to be

$$R_1(\Delta, s) = I_1(\Delta) \exp(-\bar{\alpha}(\Delta) \ln s) , \quad (5.5)$$

and analogous to $I_n = (*I_1)^n$ we define the n -reggeon propagator to be

$$R_n(s, \Delta) = (*R_1)^n(s, \Delta) , \quad (5.6)$$

then the sum (5.3), to $O(g^6)$, is equal to

$$\frac{1}{2s} T = -g^2 R_1(\Delta, s) \cdot \mathbf{G}_1 + \frac{ig^4}{2!} [R_2(\Delta, s) \cdot \mathbf{G}_2 + R_{2,1}(\Delta, s) \cdot \mathbf{G}_3] + \frac{g^6}{3!} R_3(\Delta, s) \cdot \mathbf{G}_4 . \quad (5.7)$$

The function $R_{2,1}$ is equal to

$$R_{2,1}(s, \Delta) = \frac{1}{\pi} g^2 (\ln s) \left[I_3 - \frac{1}{2} \Delta^2 I_2^2 \right] . \quad (5.8)$$

The physical interpretation of these equations will be deferred till Sec. 6.1.

5.3 Sum of Nonabelian Cut Diagrams

The QCD nonabelian cut diagrams to $O(g^6)$ are shown in Fig. 17, with a subscript ‘ c ’ to emphasize that they are cut diagrams and not Feynman diagrams. Their computations can be found in Ref. [2].

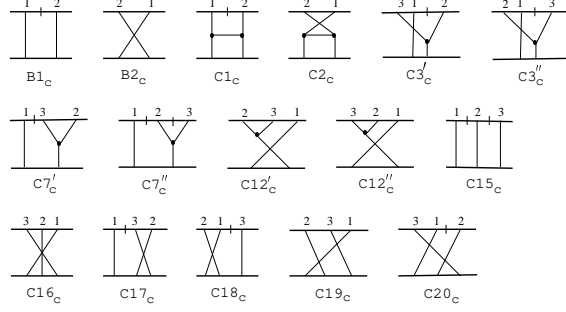


Figure 17: Nonabelian cut diagrams for QCD to order g^6 .

For the s -channel-ladder cut diagrams, the computation is straight forward and one gets their contributions to $T/(2s)$ to be

$$\begin{aligned}
B1_c &= +\frac{1}{2}ig^4 I_2 \cdot \mathbf{G}_2 \\
B2_c &= +\frac{c}{2\pi}(\ln s)g^4 I_2 \cdot c\mathbf{G}_1 \\
C15_c &= +\frac{1}{6}g^6 I_3 \cdot \mathbf{G}_4 \\
C16_c &= -\frac{c^2}{2\pi^2}(\ln s)g^6 J_3 \cdot c^2\mathbf{G}_1 \\
C17_c &= C18_c = 0 \\
C19_c &= 0 \\
C20_c &= -\frac{1}{2\pi}i(\ln s)g^6 I_3 \cdot (c\mathbf{G}_2 - \mathbf{G}_3) .
\end{aligned} \tag{5.9}$$

Similarly, we choose to cut the line of the planar diagram C1 to obtain

$$\begin{aligned}
\overline{C1}_c &= -g^4\beta i(\ln s) \left[\frac{1}{2}\Delta^2 I_2^2 - J_2 I_2 \right] \cdot \mathbf{G}_3 \\
\overline{C2}_c &= -g^2\beta^2(\ln^2 s) \left[\frac{1}{2}\Delta^2 I_2^2 - J_2 I_2 \right] \cdot c^2\mathbf{G}_1 .
\end{aligned} \tag{5.10}$$

The twelve diagrams C3 to C20 can be divided into four groups of three, each giving identical contributions, so it is necessary to consider only one of these groups. The group of C3, C7, C12 have been chosen for that purpose. There is a symmetry between gluon lines 2 and 3 so we may double this group and consider it as a sum of six Feynman diagrams. By applying the multiple commutator formula, the six cut diagrams shown in Fig. 17 are obtained. Their values are

$$\begin{aligned}
C3_c &= \frac{1}{2}(C3'_c + C3''_c) = -g^4\beta i(\ln s)\frac{1}{4}J_2 I_2 \cdot \mathbf{G}_3 \\
C7_c &= \frac{1}{2}(C7'_c + C7''_c) = 0 \\
C12_c &= \frac{1}{2}(C12'_c + C12''_c) = g^2\beta^2(\ln^2 s)\frac{1}{4}J_2 I_2 \cdot (-c^2\mathbf{G}_1) .
\end{aligned} \tag{5.11}$$

It is easy to verify that they sum up once again to (5.3) as they should.

Comparing this calculation of the cut diagrams with the earlier calculation of Feynman diagrams, one notes that

1. The coupling-constant and energy dependence $g^{2m}(g^2 \ln s)^p$, noted previously to be true for *sums of Feynman diagrams* under item ‘3’ of the last subsection, is now true for *individual* nonabelian cut diagrams. In other words, delicate cancellations of the kind found in Feynman diagrams when they are summed never appear in cut diagrams. This is one of the main advantages of dealing with nonabelian cut diagrams.
2. In leading-log approximation, functions J_2 and J_3 that appeared in individual Feynman diagrams but get cancelled in the sum never even occur here.

6 MULTIPLE REGGEONS AND QCD

6.1 The Reggeized Factorization Hypothesis

Eq. (5.7) shows that QCD scattering takes on a simple form at high energies, at least up to $O(g^6)$. The color factors present are those of Fig. 16, or equivalently Figs. 18(a), (b), (e), and (c). Interestingly enough, the spacetime amplitudes are also given by these same figures in Fig. 18, if they are interpreted as *reggeon diagrams*.

The vertical lines in Fig. 18 are reggeized gluons. The horizontal lines are the leading particles (top and bottom), or ordinary gluons produced from the reggeons. These are two-dimensional diagrams in the transverse-momentum space: the (vertical) reggeon propagators are given by $R_1(s, q_\perp)$ of (5.5), horizontal lines carry no factor, each vertex carries a factor g , and loop integrations for $-T/(2s)$ are given by the measure $-i \int d^2 q_\perp / (2\pi)^2$. The spacetime amplitude for $-T/(2s)$ from an m -reggeized-gluon (*mrg*) diagram without produced gluons (Figs. 18(a), (b), (c)) is then given by $(-i)^{m-1} g^{2m} (*R_1)^m(s, \Delta) / m! = (-i)^{m-1} g^{2m} R_m(s, \Delta) / m!$, where the factor $1/m!$ is a symmetry factor. This agrees with the terms $\mathbf{G}_1, \mathbf{G}_2, \mathbf{G}_4$ in (5.7).

For the reggeon diagram 18(e) with a produced gluon, the rule is more complicated. A Lipatov vertex $gC_\mu(q_i, q_{i+1})$ is to be placed at every reggeon-reggeon-gluon junction. For the elastic scattering diagrams in Fig. 18, they always come in a pair, so the factor is

$$\begin{aligned}
 -2g^2 \mathcal{K}(q_i, q_{i+1}) &\equiv g^2 C^\mu(q_i, q_{i+1}) C_\mu(\Delta - q_i, \Delta - q_{i+1}) \\
 &= -2g^2 \left[\Delta^2 - \frac{(\Delta - q_{i\perp})^2 q_{i+1\perp}^2 + (\Delta - q_{i+1\perp})^2 q_{i\perp}^2}{(q_{i\perp} - q_{i+1\perp})^2} \right], \quad (6.1)
 \end{aligned}$$

as shown in Fig. 19.

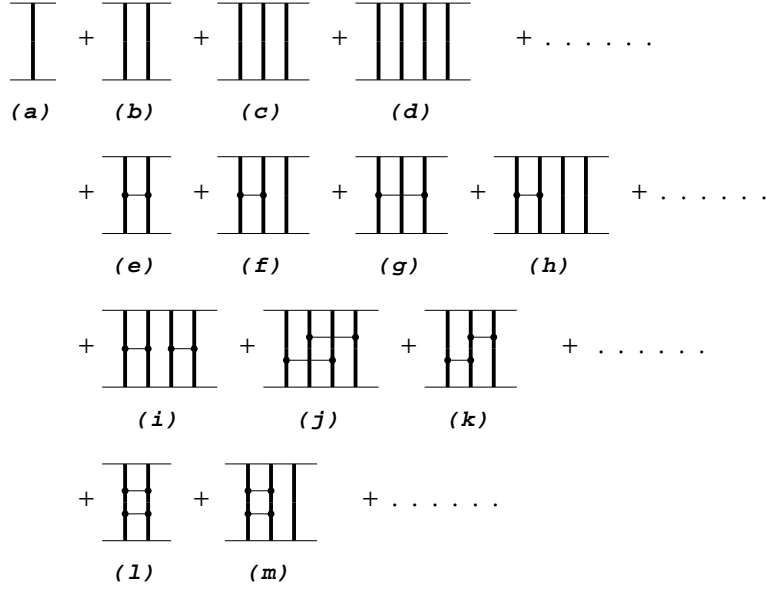


Figure 18: Reggeon diagrams for quark-quark scattering.

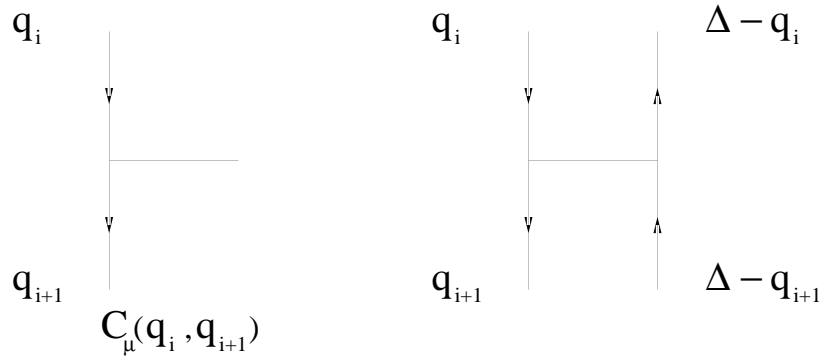


Figure 19: (a) A Lipatov vertex $gC_\mu(q_i, q_{i+1})$; (b). Two Lipatov vertices $-2g^2\mathcal{K}(q_i, q_{i+1})$.

In addition, the vertical reggeon lines should be thought of as covering the rapidity range stretched between the top leading particle and the bottom leading particle. Each horizontal line connected by two Lipatov vertices must be allowed to slide along this whole rapidity range to produce a factor $(-2\pi i)/2(2\pi)^2 \int dy \simeq -i \ln s/4\pi$ per produced gluon. In $O(g^6)$, the contribution from 18(e) to $-T/(2s)$ is therefore given by

$$\begin{aligned}
-\frac{T}{2s} &= \frac{1}{2!} \frac{-i \ln s}{4\pi} \left[\frac{-i}{(2\pi)^2} \right]^2 g^6 \int d^2 q_{1\perp} d^2 q_{2\perp} R_1(s, q_{1\perp}) R_1(s, q_{2\perp}) R_1(s, \Delta - q_{1\perp}) R_1(s, \Delta - q_{2\perp}) \cdot \\
&\cdot (-2) \mathcal{K}(q_1, q_2) \\
&\simeq \frac{-ig^6 \ln s}{8\pi} \left[\frac{-i}{(2\pi)^2} \right]^2 \int d^2 q_{1\perp} d^2 q_{2\perp} \frac{1}{q_{1\perp}^2} \frac{1}{q_{2\perp}^2} \frac{1}{(\Delta - q_{1\perp})^2} \frac{1}{(\Delta - q_{2\perp})^2} \cdot \\
&\quad (-2) \left[\Delta^2 - \frac{(\Delta - q_{1\perp})^2 q_{2\perp}^2 + (\Delta - q_{2\perp})^2 q_{1\perp}^2}{(q_{1\perp} - q_{2\perp})^2} \right] \\
&= \frac{ig^6 \ln s}{2\pi} \left(I_3 - \frac{1}{2} \Delta^2 I_2^2 \right), \tag{6.2}
\end{aligned}$$

in agreement with the \mathbf{G}_3 term of (5.7).

In the leading-log approximation where $g^2 \ll 1$ and $g^2 \ln s = O(1)$, every R_i and every \mathcal{K} are $O(1)$. Since the produced gluons must slide along the whole rapidity range mapped out by the reggeon lines, whenever one of them appears a factor $g^2 \ln s = O(1)$ is produced. Hence an mrg amplitude is of order g^{2m} , whether there are produced gluons or not. This is certainly true in (5.7) but it should also be generally true for all reggeon diagrams in Fig. 18.

This picture of reggeized exchange is simple and elegant, but does this $O(g^6)$ result generalize to all orders? In other words, can the sum of all high-energy elastic scattering Feynman diagrams be factorized into reggeon diagrams like those in Fig. 18? If it does, is the reggeon still given by (5.4) to all orders, or something more complicated is required? We shall refer to the affirmative answer to both of these questions as the *reggeized factorization hypothesis*.

As discussed above, this hypothesis is completely verified to $O(g^6)$. It has also been partially checked to $O(g^8)$ and $O(g^{10})$ [8]. The main focus of this section is to ask whether this is true to higher orders. To be sure, we do not know the full answer at the present but some partial answers are known. For example, using the technique of nonabelian cut diagrams, we can show that the hypothesis is correct at least for s -channel-ladder diagrams. This will be discussed in Sec. 6.4. Before doing that, we shall go over briefly what has been known for some time about multiple reggeon exchanges.

6.2 BFKL Equation and Unitarity

By summing t -channel-ladder diagrams in the leading-log approximation one obtains the result that the octet channel is dominated by a reggeized gluon exchange, with a regge trajectory given by $\alpha(t) = 1 + \bar{\alpha}(\Delta)$, where $\bar{\alpha}(\Delta)$ is given in (5.4). The propagator of this reggeized gluon is given by (5.5). [8, 9].

The 2rg (two-reggeized-gluon) exchanges come from the sum of t -channel-reggeon-ladder diagrams [9]. These are diagrams in which n ordinary gluons are produced and absorbed by two reggeized gluons. They are illustrated in Fig. 18 by diagrams (b), (e), and (l) respectively for $n = 0, 1, 2$.

In the leading-log approximation, the produced gluons are strongly ordered in rapidity, hence the rungs of the ladder do not cross. A diagram with n produced gluons has $n + 1$ transverse integrations. The integrand consists of n factors of \mathcal{K} and $2(n + 1)$ reggeon propagators R_1 . Its amplitude has been computed in the following way [9]. First, its discontinuity is calculated from the Cutkosky rules. Then the whole amplitude is computed using s -channel dispersion relations.

The color-octet amplitude for quark-quark scattering is predominantly real, and its leading contribution is given by the 1rg (one reggeized gluon exchange) diagram. However, this real part should also be obtainable from the imaginary part computed in the 2rg Cutkosky diagram via a dispersion relation. Explicit calculation shows that this is indeed the case.

The color-singlet amplitude is the Pomeron amplitude originally proposed by Low and Nussinov [13]. It is predominantly imaginary, a factor g^2 down from the color-octet amplitude, and dominated by the 2rg diagrams in the leading-log approximation. Its computation is fairly difficult [9], and it leads to a total cross-section growing like S^A , with $A = g^2(\ln 2)N_c/\pi^2$. This violates the Froissart bound and unitarity, hence the computation as it stands must be incomplete. Subleading-log contributions must be added to unitarize it. These may be the subleading-log contributions from the same t -channel-reggeon-ladder diagrams, or the leading-log contributions from diagrams associated with more reggeon exchanges, or both.

Subleading-log contributions from Feynman diagrams are very difficult to compute, so if we must do it that way there would be very little hope of obtaining any result except in very low orders. However, if we sum up all multiple reggeon exchange diagrams as in Fig. 18, then formally s -channel unitarity is restored. From the discussion at the end of the last subsection, we know that an mrg amplitude is of order g^{2m} , so multiple reggeon diagrams computed to leading-log approximation do contribute to subleading-logs of the Pomeron amplitude. Thus there is a hope of unitarizing the Pomeron amplitude by including all these multiple reggeon diagrams computed to leading-log approximation, provided the reggeized factorization hypothesis is correct.

6.3 Nonabelian Cut Diagrams vs Feynman Diagrams

We saw in the $O(g^6)$ computation of Sec. 5 that delicate cancellations occur in the sum of Feynman diagrams, making it necessary to compute individual Feynman diagrams to subleading accuracies in order to obtain a finite sum. In contrast, this never happens in nonabelian cut diagrams, so they can be computed simply to the leading order, a much easier task. We shall argue below that this situation is true to all orders provided the reggeized factorization hypothesis is correct.

Recall that for nonabelian cut diagrams the color factor is computed from the comple-

mentary cut diagrams. For a diagram to contribute to an m rg amplitude, it must have m uncut propagators on the upper tree, which means that the corresponding cut diagrams from which the spacetime amplitude is computed must have m cut lines.

Now an ℓ -loop amplitude can grow at most like $(\ln s)^\ell$. However, each cut propagator with its δ -function will deprive that loop of a $\ln s$ factor because it replaces integrations like $\int_e dx/x \sim \ln s$ by $-2\pi i \int dx \delta(x) \sim 1$. A diagram with m cuts is thus deprived of at least m factors of $\ln s$, making it grow at best like $g^{(2m)}(g^2 \ln s)^p$, for a diagram of order $2(m+p)$. Since $g^2 \ln s = O(1)$, this is of order g^{2m} , precisely what an m rg amplitude requires, so it is sufficient to compute each nonabelian cut diagrams just to the leading order.

In contrast, the corresponding Feynman diagram has no cut in its spacetime part nor its color part. Its color factor will generally involve n rg diagrams with $n \geq m$. If this diagram contributes to an n rg diagram without delicate cancellation then its spacetime amplitude must be deprived of more (since $n \geq m$) factors of $\ln s$. On the other hand, without cuts in the spacetime diagram, there is no guarantee to have any deprivation of $\ln s$ at all. The absence of cuts in both therefore conspire to render too many $\ln s$ factors compared to those needed for reggeon amplitudes. In order for the reggeized factorization hypothesis to be valid, delicate cancellations are then necessary in the sum to reduce the $\ln s$ powers.

This argument shows that nonabelian cut diagrams are much more suitable for the computation of sums than Feynman diagram. In fact, there is virtually no hope of obtaining sums in higher orders by computing Feynman diagrams individually.

6.4 s -Channel-Ladder Diagrams

In this subsection we outline the computation of the s -channel ladder diagrams to show that they satisfy the reggeized factorization hypothesis. For details of the arguments see Ref. [10]. For reasons discussed in the last subsection, we will use nonabelian cut diagrams rather than Feynman diagrams in our computation.

The Feynman diagrams are the same diagrams as those computed in Sec. 3.2 for QED to obtain an eikonal amplitude, leading to a constant total cross-section in that case. The situation in QCD is quite different. We know from the $O(g^6)$ computation in Sec. 5 that there are $\ln s$ factors present even for the Pomeron amplitude, so the total cross-section is no longer constant in QCD.

There is another important difference. The sum of these ladder diagrams in QED is gauge invariant but that in QCD is not. To make it gauge invariant we virtually have to include all diagrams, and that computation is very difficult. What appears below is the result in the Feynman gauge.

We shall consider quark-quark scattering in which the ‘quarks’ carry an arbitrary color in an $SU(N_c)$ theory. Since spin is unimportant at high energies, what is thus obtained is valid for gluon-gluon scattering as well. The two quarks will be represented by two horizontal lines, and the n exchanged gluons by vertical or slanted lines as in Fig. 20 for $n = 4$.

We shall choose the *planar diagram* to be the one in which all propagators on the upper line are cut, as shown in Fig. 20(a). This can be accomplished by numbering the gluons in

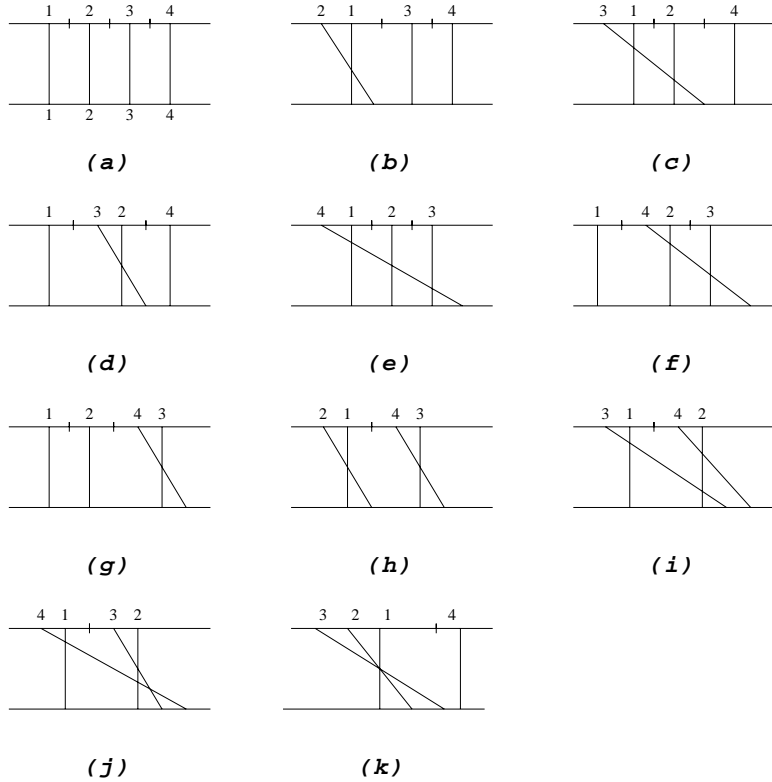


Figure 20: s -channel-ladder cut diagrams for $n = 4$.

the manner shown. For convenience we shall also draw the gluons of the planar diagram as vertical lines.

All the other nonabelian cut diagrams can be obtained by pulling the upper ends of a number of gluon lines leftward, in all possible combinations. The propagator to the right of a slanted line is uncut, and the propagators to the right of a vertical line is cut. See Fig. 20. This is so because once the upper end of a gluon line is moved leftward, there will always be another gluon with a smaller number to its right.

We shall refer to these s -channel-ladder cut diagrams as SC diagrams. Their complementary diagrams used to compute color factors will be referred to as SCC diagrams.

As discussed in the last subsection, a nonabelian cut diagram with m cuts are deprived of at least m would-be $\ln s$ factors. Such a diagram is said to be *saturated* if it is deprived of exactly m factors of $\ln s$, and no more. The leading contribution to a m rg diagram will come only from the saturated SC diagrams with m cuts.

By referring to the computations in Secs. 2.2.3 and 2.2.4, we see that even diagrams with no cuts may not get its full share of $\ln s$ factors – Fig. 4 does but Fig. 5 does not. Like the cases in Figs. 4 and 5, an SC diagram is saturated iff it does not have two consecutive uncut propagators on the upper line. Thus 20(k) is not saturated, but every other diagram in Fig. 20 is.

We outline now the procedure for computing sums of SC diagrams of any n . For details please consult Ref. [10].

We shall refer to color factors of the type shown in Fig. 18 as *regge color factors*. Given an SCC diagram, the first step is to use eqs. (1.8) and (1.9), or equivalently the graphical rules in Fig. 1, to decompose its color factor into a sum of regge color factors. We will call a regge color factor *primitive* if it remains connected after the top and bottom lines are removed. Thus the regge color factors in Figs. 18(a), 18(e), 18(k), and 18(l) are primitive, but none of the others explicitly shown in Fig. 20 are. 18(l) and 18(m) do not occur in SCC diagrams so we will ignore them. The other three primitive ones 18(a), (e), and (k) will respectively be named H_0 , H_1 , and H_2 . It can be shown that the only primitive regge color factors entering into SCC diagrams are H_p ($p = 0, 1, 2, 3, \dots$), representing a pattern with p horizontal steps climbing up from left to right.

It can also be shown that regge color factors with the same primitive components can be identified in the leading-log approximation. For that reason a regge color factor can simply be labelled by the number of each primitive component it contains, *i.e.*, can be expressed in the form $\Phi = \prod_{p=0}^{\infty} H_p^{f_p}$. For example, the color factors of 18(b), (c), (d) are H_0^2 , H_0^3 , and H_0^4 respectively. The others are 18(f) = 18(g) = $H_0 H_1$, 18(h) = $H_0^2 H_1$, 18(i) = 18(j) = H_1^2 .

The next step is to collect all SC diagrams contributing to a given regge color factor Φ . It turns out that these diagrams can be summed up using the factorization theorem (3.3) to be ($\mathcal{A} = -T/2s$)

$$\mathcal{A}\{\Phi\}(\Delta) = \prod_{p=0} (-i)^{f_p-1} [* \mathcal{A}\{H_p\}]^{f_p} (\Delta) , \quad (6.3)$$

where $\mathcal{A}\{H_p\}$ is the sum of all SC amplitudes whose corresponding SCC diagrams contain the connected primitive color factor H_p . This shows that the reggeized factorization hypothesis holds for all s -channel-ladder diagrams.

In particular, $\mathcal{A}\{H_0\}(\Delta)$ is simply $g^2 R_1(s, \Delta)$, where R_1 is given by (5.5) to order g^2 . The g^4 contribution comes from diagrams $C1_c$ and $C2_c$ of Fig. 17 and they are not SC diagrams.

Using (5.6), the \mathbf{G}_2 and \mathbf{G}_4 amplitudes of (5.7) are special cases of (6.3) with $f_0 = 2, 3$ and all other $f_p = 0$.

Similarly, $\mathcal{A}\{H_1\}(\Delta) = (-i/2)R_{2,1}(s, \Delta)$, where $R_{2,1}$ is given by the first term of (5.8) – the second term there does not come from SC diagrams.

Acknowledgements

This research is supported in part by the by the Natural Science and Engineering Research Council of Canada, and the Fonds pour la Formation de Chercheurs et l'Aide à la Recherche of Québec. I would like to thank my collaborators Yong-Jian Feng, Omid Hamidi-Ravari, and Keh-Fei Liu. I am specially grateful to Yong-Jian Feng for drawing the extra diagrams in these notes.

References

- [1] C.S. Lam and K.F. Liu, McGill/96-12=hep-ph/9604377, to appear in *Nucl. Phys. B*.

- [2] Y.J. Feng, O. Hamidi-Ravari, and C.S. Lam, *Phys. Rev. D* **54** (1996) 3114 (McGill/96-13=hep-ph/9604429).
- [3] G. 't Hooft, *Nucl. Phys.* **B72** (1974) 461; E. Witten, *Nucl. Phys.* **B160** (1979) 57; S. Coleman, Erice Lectures (1979).
- [4] R.F. Dashen, E. Jenkins and A.V. Manohar, *Phys. Rev. D* **49** 4713; M.A. Luty and J. March-Russell, *Nucl. Phys.* **B426** (1994) 71.
- [5] C.S. Lam, in 'Proceedings of the International Symposium on Heavy Flavor and Electroweak Theory', Aug. 1995, Beijing, *Eds: C.H. Chang and C.S. Huang*, World Scientific (1996) (McGill/96-22=hep-ph/9606350); C.S. Lam and K.F. Liu, to be published.
- [6] H. Cheng and T.T. Wu, '*Expanding Protons: Scattering at High Energies*', (M.I.T. press, 1987).
- [7] H. Cheng and T.T. Wu, *Phys. Rev.* 186 (1969) 1611; M. Levy and J. Sucher, *Phys. Rev.* 186 (1969) 1656.
- [8] C.Y. Lo and H. Cheng, *Phys. Rev.* D13 (1976) 1131; D15 (1077) 2959; H. Cheng, J.A. Dickinson, and K. Olaussen, *Phys. Rev.* D23 (1981) 534.
- [9] L.N. Lipatov, *Yad. Fiz.* 23 (1976) 642 [*Sov. J. Nucl. Phys.* 23 (1976) 338]; Ya. Ya. Balitskii and L.N. Lipatov, *Yad. Fiz.* 28 (1978) 1597 [*Sov. J. Nucl. Phys.* 28 (1978) 822]; E.A. Kuraev, L.N. Lipatov, and V.S. Fadin, *Zh. Eksp. Teor. Fiz.* 71 (1976) 840 [*Sov. Phys. JETP* 44 (1976) 443]; *ibid.* 72 (1977) 377 [*ibid.* 45 (1977) 199]; L.N. Lipatov, in 'Perturbative Quantum Chromodynamics' (A.H. Mueller, ed., World Scientific 1989); V. Del Duca, hep-ph/9503226.
- [10] Y.J. Feng and C.S. Lam, McGill/96-19=hep-ph/9606351.
- [11] C.S. Lam, McGill/96-23=hep-ph/9606374.
- [12] Y.J. Feng and C.S. Lam, *Phys. Rev.* D50 (1994) 7430.
- [13] F.E. Low, *Phys. Rev.* D12 (1975) 163; S. Nussinov, *Phys. Rev. Lett.* 34 (1975) 1286.